The EMBO Journal (2009) 28, 1001–1015 | © 2009 European Molecular Biology Organization | All Rights Reserved 0261-4189/09
www.embojournal.org

THE EMBO JOURNAL

SRBC/cavin-3 is a caveolin adapter protein that regulates caveolae function

Kerrie-Ann McMahon[1], Hubert Zajicek[1], Wei-Ping Li[1], Michael J Peyton[2,3], John D Minna[2,3], V James Hernandez[1], Katherine Luby-Phelps[1] and Richard GW Anderson[1,*]

[1]Department of Cell Biology, University of Texas Southwestern Medical Center, Dallas, TX, USA, [2]Department of Internal Medicine, University of Texas Southwestern Medical Center, Dallas, TX, USA and [3]Hamon Center for Therapeutic Oncology Research, University of Texas Southwestern Medical Center, Dallas, TX, USA

Caveolae are a major membrane domain common to most cells. One of the defining features of this domain is the protein caveolin. The exact function of caveolin, however, is not clear. One possible function is to attract adapter molecules to caveolae in a manner similar to how clathrin attracts molecules to coated pits. Here, we characterize a candidate adapter molecule called SRBC. SRBC binds PKCδ and is a member of the STICK (substrates that interact with C-kinase) superfamily of PKC-binding proteins. We also show it co-immunoprecipitates with caveolin-1. A leucine zipper in SRBC is essential for both co-precipitation with caveolin and localization to caveolae. SRBC remains associated with caveolin when caveolae bud to form vesicles (cavicles) that travel on microtubules to different regions of the cell. In the absence of SRBC, intracellular cavicle traffic is markedly impaired. We conclude that SRBC (sdr-related gene product that binds to c-kinase) and two other family members [PTRF (Pol I and transcription release factor) and SDPR] function as caveolin adapter molecules that regulate caveolae function.

The EMBO Journal (2009) **28,** 1001–1015. doi:10.1038/emboj.2009.46; Published online 5 March 2009
Subject Categories: membranes & transport
Keywords: caveolae; caveolin; endocytosis; adapter protein

Introduction

Caveolae are the most abundant membrane domain on the cell surface devoted to endocytosis. They can occupy 18–40% of the plasma membrane surface (Chang *et al*, 1994) and engage in at least three different types of dynamic activities (Mundy *et al*, 2002; White and Anderson, 2005). Type 1 caveolae are able to pinch off the membrane to form endocytic vesicles called cavicles (Mundy *et al*, 2002) that can carry cargo such as SV40 virus to specialized endosomes called caveosomes (Pelkmans *et al*, 2001). Cavicles can also travel to the recycling endosome region of the cell (Mundy *et al*, 2002). Cavicle movement to these sites is microtubule dependent. Type 2 caveolae, which are the most abundant type, superficially appear not to be dynamic (Thomsen *et al*, 2002). Recent studies suggest, however, that quantal units of caveolae are engaged in continuous rounds of fission and fusion at the cell surface (Pelkmans and Zerial, 2005). Quantal caveolae behaviour exhibits the same kinetics and characteristics as folate receptor internalization and recycling by potocytosis (Anderson *et al*, 1992), which is a caveolae-dependent mechanism for delivering vitamins and ions such as calcium (Isshiki *et al*, 2002) to the cell interior. Type 2 cavicles can also move rapidly just beneath the membrane. The third type of caveolae behaviour (type 3) is the relatively uncharacterized ability of these domains to form long, thin caveolin-1 (Cav1)-positive tubules that project from the plasma membrane deep into the cell interior (Mundy *et al*, 2002). There are no known functions for these tubules, but GPI-anchored prions have been localized to these structures by immunogold electron microscopy (EM) (Peters *et al*, 2003). Type 3 caveolae may mediate Cav3-rich tubule formation during skeletal muscle cell development (Parton *et al*, 1997). All three types of caveolae behaviours can occur in the same cell.

The three pathways depend on the ability of caveolae to form flask or tubular invaginations and, at least for types 1 and 2, seal off from the extracellular space. Several years ago we initiated a search for molecules that control caveolae internalization and identified PKCα as a regulator of type 2 caveolae internalization (Smart *et al*, 1995a). PKCα is highly enriched in caveolae (Smart *et al*, 1995a), and deletion of PKCα from cells or displacement from caveolae by AlF_4 or inactivation with inhibitors (Mineo and Anderson, 2001) blocks uptake of folate receptors and flattens the flask-shaped morphology of caveolae. PKCα is probably a natural regulator of caveolae internalization because activation of histamine H1 receptors, which causes the dissociation of PKCα from caveolae, transiently blocks folate internalization (Smart *et al*, 1995a). Phosphorylation of an unidentified 90-kDa protein by PKCα has been linked to caveolae internalization. On the basis of these observations, we hypothesized that caveolae contain a protein(s) that recruits PKCα to this domain. Subsequently, we identified SDR (serum deprivation response) protein as a PKCα-binding protein that is enriched in caveolae (Mineo *et al*, 1998). PKCα binding to SDR in caveolae is dependent on amino acids 145–250 of SDR, calcium and an intact PKC regulatory domain. Addition of phosphatidylserine (PS) is not required.

SDR (also called PS-p68 and SDPR) is a 412-amino-acid modular protein that contains a leucine zipper (LZ), a PKC-binding site, a PKC phosphorylation site, a PS-binding site and two PEST domains. These structural motifs are also found in PTRF [Pol I and transcription release factor (Jansa *et al*, 1998), also called, cavin/cav-p60 (Voldstedlund *et al*, 2003; Vinten *et al*, 2005)] and SRBC [sdr-related gene product that binds to c-kinase (Izumi *et al*, 1997)]. On the basis of

*Corresponding author. Department of Cell Biology, University of Texas Southwestern Medical Center at Dallas, 5323 Harry Hines Blvd, Dallas, TX 75390-9039, USA. Tel.: +1 214 648 2346; Fax: +1 214 648 7577; E-mail: richard.anderson@utsouthwestern.edu

Received: 1 August 2008; accepted: 21 January 2009; published online: 5 March 2009

these motifs, these three proteins form a subset of the STICK (substrates that interact with C-kinase) superfamily of PKC-binding proteins (Chapline *et al*, 1998; Jaken and Parker, 2000)). In addition to PKC-binding sites, all STICK proteins contain PS-binding sites and are found at the interface between membranes and the cytoskeleton. They include MARCKS, annexin I and II, desmoykin, vinculin/talin, α- and β-adducin, GAP43 and AKAP79.

Recently, PTRF was reported to be concentrated in adipocyte (Vinten *et al*, 2005; Aboulaich *et al*, 2006; Hill *et al*, 2008; Liu and Pilch, 2008) and smooth muscle caveolae (Voldstedlund *et al*, 2003), even though it was originally identified and studied as a transcription release factor (Jansa *et al*, 1998, 2001; Jansa and Grummt, 1999; Hasegawa *et al*, 2000). PTRF has also been implicated in regulating caveolae function (Hill *et al*, 2008; Liu and Pilch, 2008).

In contrast to SDPR and PTRF, a relationship between SRBC and caveolae function has not been established. SRBC was initially identified in overlay assays as a PKCδ-binding protein (Izumi *et al*, 1997). PKCδ binds and phosphorylates SRBC *in vitro*. Similar to SDPR, the mRNA for SRBC is induced in response to serum deprivation as well as during retinoic acid-induced differentiation of P19 cells. SRBC was also identified in a yeast two-hybrid screen as a BRCA1-interacting protein (Xu *et al*, 2001). The human SRBC gene maps to 11p15.5–15.4, which is a suppressor region that is mutated in a number of sporadic breast, lung and ovarian cancers. The loss of SRBC in these cancers appears to be caused by DNA methylation and subsequent gene silencing. A follow-up study (Zochbauer-Muller *et al*, 2005) suggests, however, that DNA methylation is not the only mechanism of SRBC loss in lung cancer cells. SRBC is also downregulated in gastric cancer (Lee *et al*, 2007). A naturally occurring fusion protein isolated from colon cancer cells, which consists of the first 184 amino acids of SRBC linked to c-Raf, has cell-transforming activity (Tahira *et al*, 1987). Interestingly, activation of c-Raf occurs in caveolae (Mineo *et al*, 1996) and Raf fused to the C-terminal consensus sequence for prenylation is constitutively active in this domain (Mineo *et al*, 1997). It is possible, therefore, that the SRBC–Raf fusion protein inappropriately targets c-Raf to caveolae where it is constitutively active.

Here, we report that SRBC is highly localized to caveolae. Targeting of SRBC to caveolae depends on both the LZ domain of SRBC and the expression of Cav1. SRBC is downregulated in response to depletion of Cav1, suggesting that Cav1 stabilizes SRBC. Spinning disc confocal microscopy shows that SRBC is in caveolae, cavicles and caveosomes and traffics with Cav1 to different locations in the cell. In the absence of SRBC, however, intracellular cavicle traffic is markedly impaired.

Results

SRBC was identified in a proteomic screen for proteins enriched in detergent-free caveolae, purified from various cell types (Aboulaich *et al*, 2004; McMahon *et al*, 2006). Alternative splicing of the mRNA for SRBC can potentially produce five different transcripts. The domain organization of these five proteins is shown in Figure 1A. The isoform used in the current study is hSRBCβ, which codes for a 261-amino-acid-long protein designated hSRBC (Izumi *et al*, 1997). All five isoforms are predicted to be soluble proteins.

We used immunofluorescence and immunogold EM to verify that SRBC is enriched in caveolae. The SRBC mAb we used is directed against the C-terminal end of hSRBCα,β (Figure 1A, bracket, hSRBCβ) and recognizes only human SRBC. This antibody, which detects a single 45-kDa band on immunoblots, colocalizes with Cav1 (Figure 1B–F). The scatter plot (Figure 1D) shows the red and green intensities at each pixel. From these data, we calculated the Pearson's coefficient of correlation (PCC), which measures how well two fluorescent foci coincide (Costes *et al*, 2004), to be 0.88 where 1.0 represents perfect colocalization. Another measure of coincidences of the two signals is the colocalization channel (Figure 1F), which is a *z*-axis projection showing voxels that have a statistically significant colocalization. Finally, immunogold labelling (Figure 1G) showed a high degree of gold localization to invaginated caveolae as well as endosomal structures that could be either caveosomes or cavicles. Substitution of an irrelevant mAb for α-SRBC IgG did not give labelling (data not shown). Therefore, hSRBC is preferentially associated with caveolae as well as caveolae-derived endo-membranes. hSRBC is localized to caveolae in many different human tissue culture cell lines (data not shown).

Tissue distribution of SRBC

We used immunofluorescence to identify tissues that express both hSRBC and Cav1 and determine whether they were both in the same cell type. Samples of human skeletal muscle, liver, stomach, lung, kidney and heart were processed for indirect immunofluorescence (Figure 2). Both proteins were expressed in all the tissues we examined, but not in every cell type within an individual tissue. For example, blood vessels expressed both proteins (yellow in the merge) in skeletal muscle tissue, whereas muscle cells *per se* expressed Cav1 but not SRBC (red in merge). In stomach, connective tissue cells expressed both proteins but neither protein was expressed in epithelium. Importantly, even though many cells expressed Cav1 but not hSRBC (red in the merge images of skeletal, liver, lung and kidney), rarely did we find cells that expressed only SRBC. This raises the possibility that SRBC expression may be linked to Cav1 expression.

LZ is required for targeting to caveolae

We used site-directed mutagenesis to identify regions of SRBC that might be necessary for targeting the protein to caveolae (Figure 3). There are at least four regions that could be involved in targeting (Figure 3A); a LZ (aa 22–70), two PEST domains (aa 140–173 and 225–241), a putative PS-binding site (aa 113–124) and a PKC-interacting region (aa 175–194). We constructed five cDNAs coding for wild type (WT) and mutant hSRBC tagged with HA. Each cDNA was expressed in human fibroblasts and the samples were processed to localize HA (green) and endogenous Cav1 (red). As expected, the WT HA–SRBC colocalized with Cav1 (Figure 3B, WT coloc) with a PCC of 0.74. Deletion of the LZ shifted hSRBC from caveolae to the cytoplasm and nucleus of the cell (Figure 3C), giving a PCC of −0.08, which indicates no specific association with Cav1. By contrast,

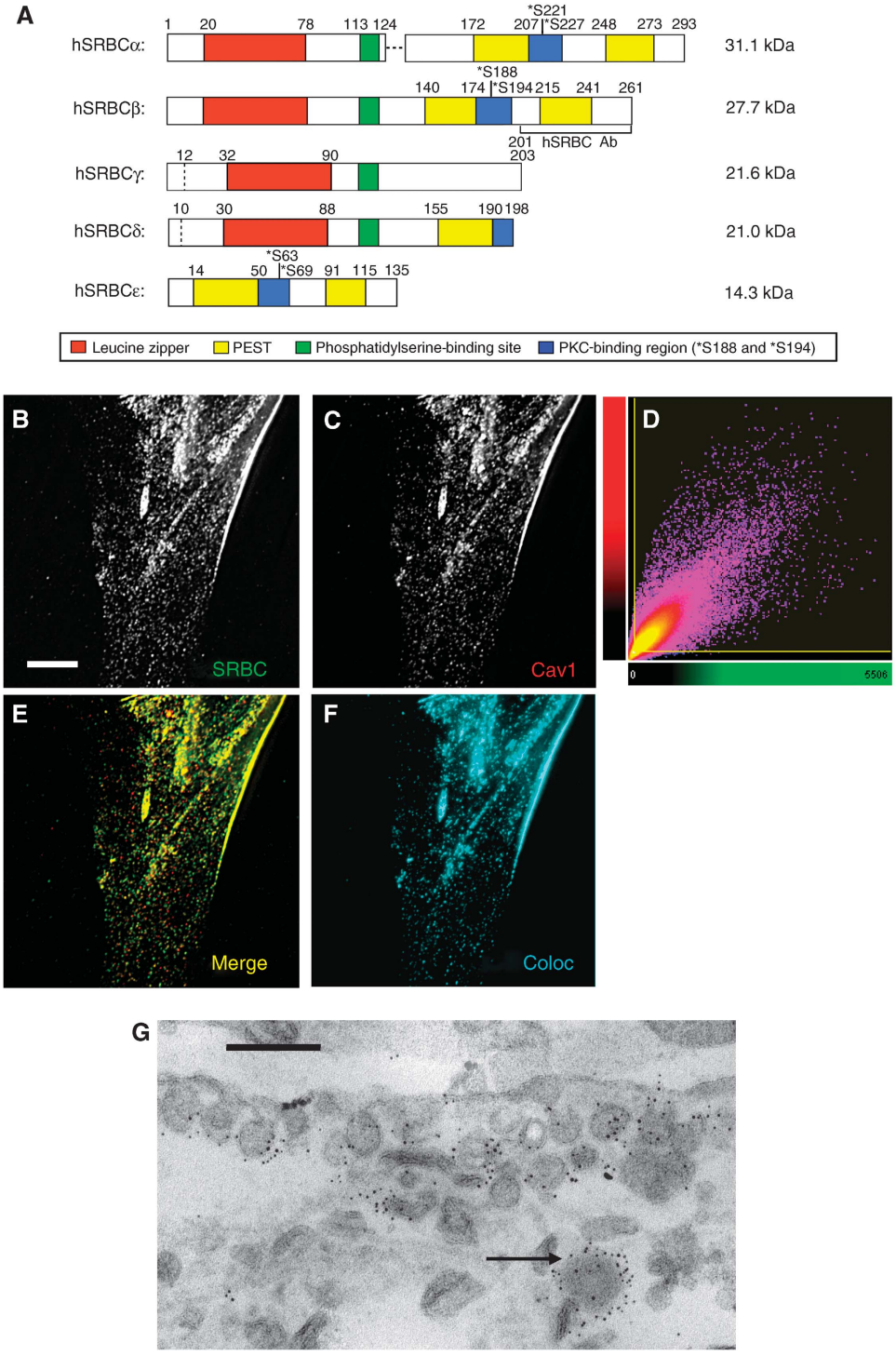

Figure 1 hSRBC is localized to human fibroblast caveolae. (**A**) The domain structure of five predicted isoforms of human SRBC. Only hSRBCβ was used in this study. The region used to produce the mAb α-SRBC is indicated in brackets. (**B–F**) Immortalized human fibroblasts were fixed, permeabilized and processed for immunofluorescence to colocalize endogenous hSRBC and Cav1 using an mAb α-hSRBC IgG (B) and pAb α-Cav1 (C). The merged image (E) and the scatter plot (D) show that greater than 88% of α-SRBC and α-Cav1 IgG spots coincide. The colocalization channel (F) is a *z*-axis projection showing voxels with statistically significant colocalization. Bar = 10 μm. (**G**) Normal human fibroblasts were processed for immunogold staining with mAb α-SRBC IgG. The majority of the gold particles was associated with invaginated caveolae at the cell surface or cavicles/caveosomes within the cell (arrow). Bar = 0.2 μm.

deletion of the PS-binding site (Figure 3D) or the PKC-binding region (Figure 3E) or the PEST domain between amino acids 215–241 (Figure 3F) had little affect on colocalization (coloc) with caveolin. The PCC for these constructs was 0.63, 0.61 and 0.78, respectively.

To determine the general importance of LZ in targeting this family of proteins to caveolae, we studied SDPR (Figure 4A). Similar to hSRBC, SDPR colocalizes with Cav1 (Figure 4B; Supplementary Figure 1SA) and both hSRBC and SDPR colocalize with each other (Supplementary Figure 1SB). The

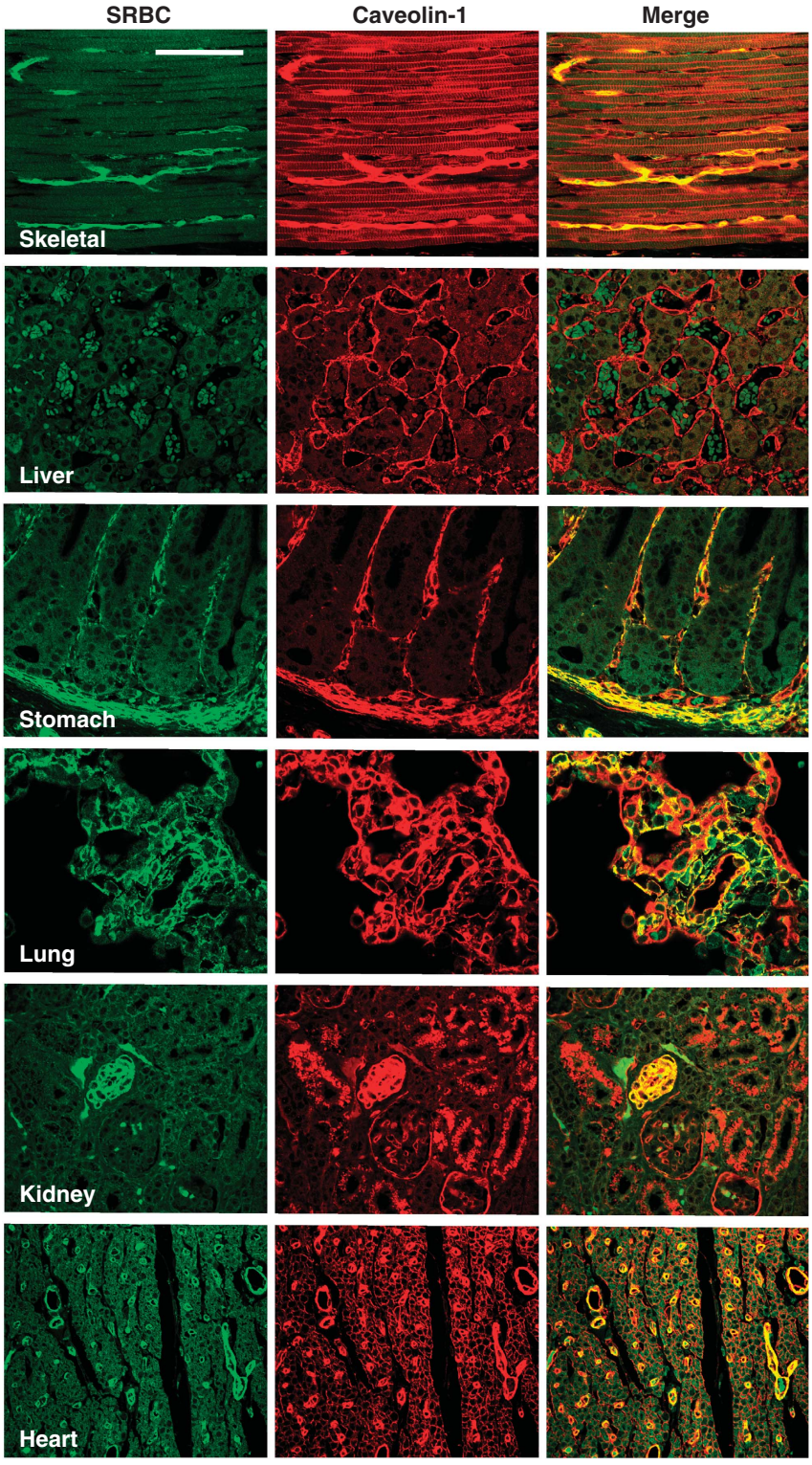

Figure 2 hSRBC and Cav1 expression in tissue cells. Sections of paraffin-embedded normal human tissues were incubated overnight at 4°C in the presence of mAb α-hSRBC IgG and pAb α-Cav1 IgG. The sections were then washed and the primary antibody was detected by incubating the sections with the appropriate Alexa-Fluor IgG. Images were taken using a Leica TCS SP confocal microscope (Leica, Bannockburn, IL). Bar = 100 μm.

LZ occupies the same relative position in SDPR (amino acids 52–100), PTRF (amino acids 50–98) and hSRBC (Figure 4A). First, we constructed cDNAs that code for amino acids 1–337 (WT), 1–168 and Δ52–100, all tagged with HA, and expressed them in human fibroblasts. The WT (Figure 4B, WT) and the 1–168 construct (Figure 4C, 1–168) localized to caveolae. The SDPR construct lacking the LZ domain, by contrast, was found in the cytoplasm and nucleus of the cell but did not colocalize with Cav1 (Figure 4D, 52–100, PCC = –0.236). Likewise an SDPR with leucines 86, 93 and 100 changed to glutamic acid did not colocalize with Cav1 (Supplementary Figure 1SC). These results suggest that the LZ has a critical

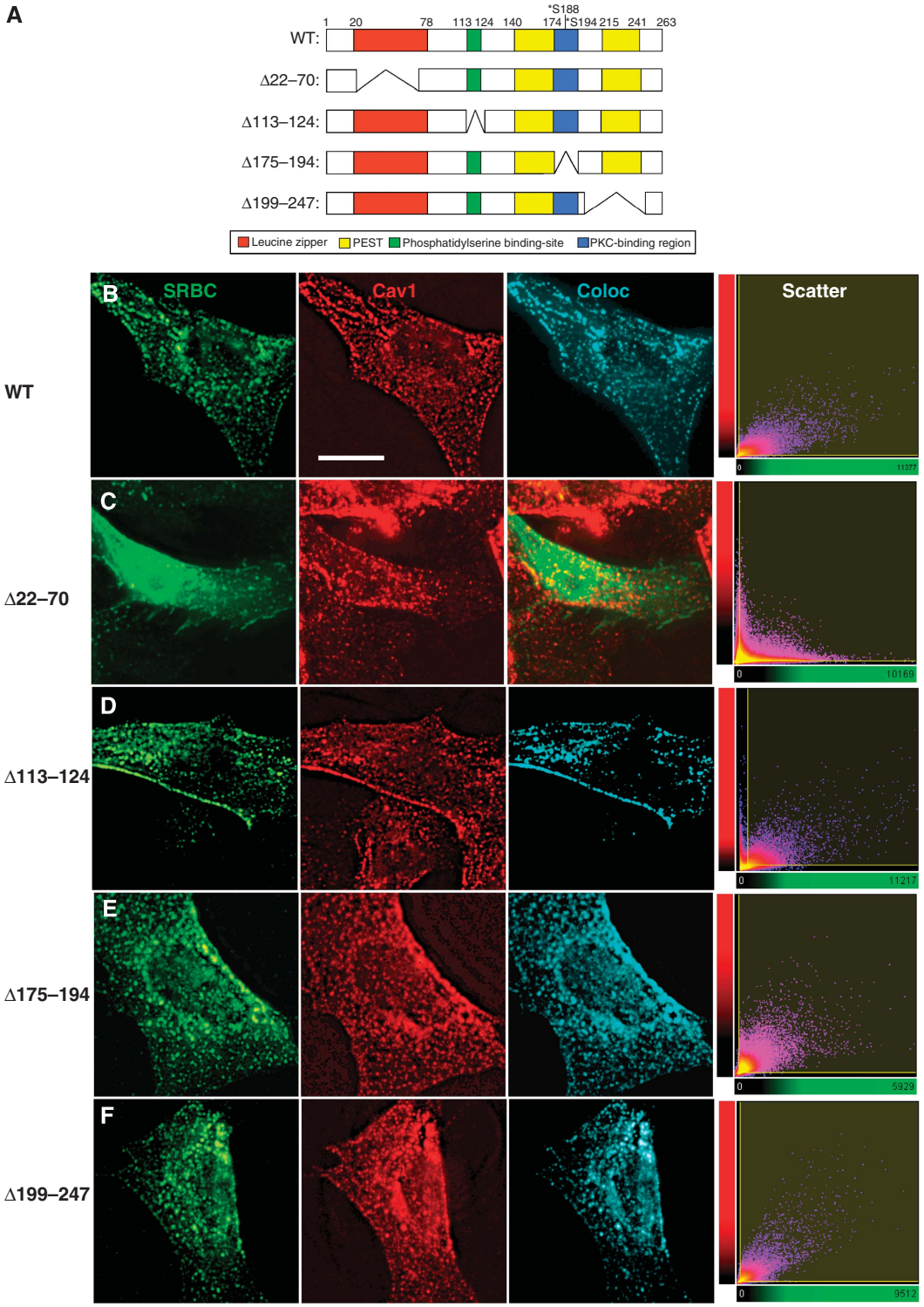

Figure 3 Leucine zipper required for hSRBC targeting to caveolae. (**A**) A diagram showing schematically the wild type and four different hSRBCs with deletions of regions that might be involved in targeting to caveolae. (**B–F**) The indicated HA-tagged versions of each construct were transiently expressed in immortalized human fibroblasts. Cells were fixed, permeabilized and processed for colocalization of Cav1 and HA using mAb α-HA and pAb α-Cav1. In (B, D–F), the fluorescence signal for the two antibodies was analysed to map voxels that overlapped between channels (coloc) as well as determine the Pearson's coefficient of correlation of the two images (PCC). Instead of using the colocalization channel for Δ22–70, we show the merge because of the diffuse distribution of the expressed protein. Bar = 10 μm.

function in directing SDPR, hSRBC and probably PTRF to caveolae and raises the possibility that other LZ-containing molecules spend time in caveolae. Dimerization of the LZ may be required for targeting.

Caveolin 1 or 3 is required for localization of hSRBC to the cell surface

Cav1 is an obvious candidate for the protein that attracts hSRBC to caveolae. We used immunofluorescence to explore

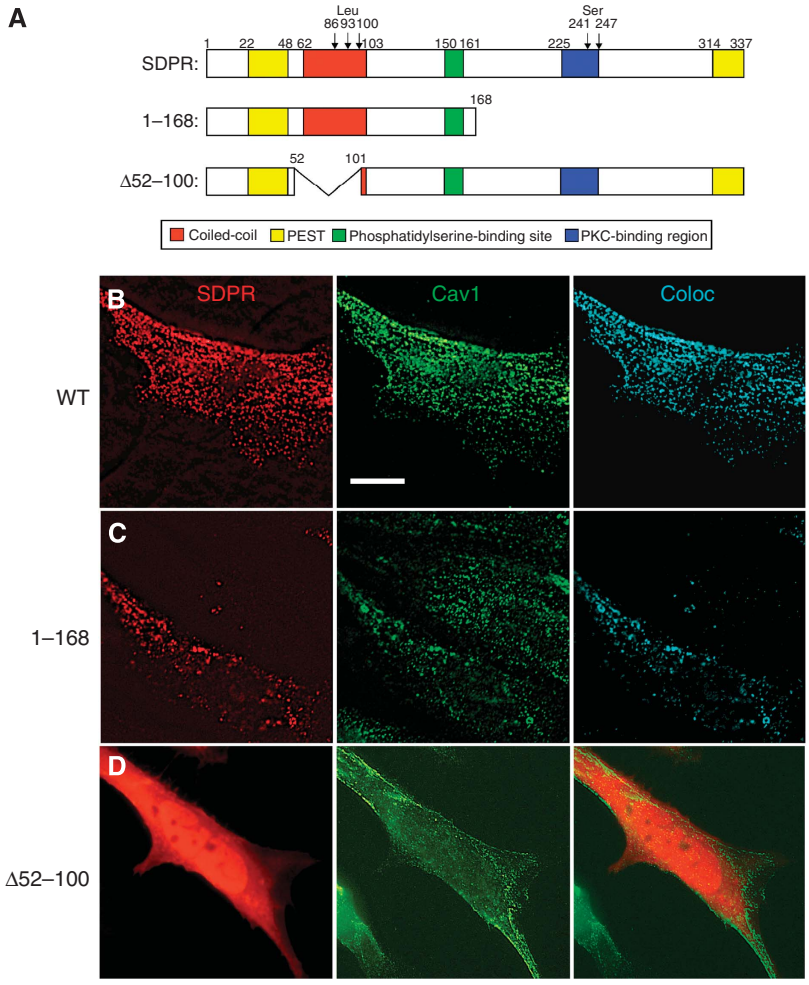

Figure 4 LZ in SDPR also required for targeting to caveolae. (**A**) A diagram showing schematically the wild type and two different deletions we made to determine the part of SDPR that was required for targeting to caveolae. (**B–D**) The indicated Myc-tagged versions of each construct were transiently expressed in immortalized human fibroblasts. Cells were fixed, permeabilized and processed for colocalization of endogenous Cav1 and Myc using mAb α-Myc and pAb α-Cav1. Instead of using the colocalization channel for Δ52–100, we show the merge because of the diffuse distribution of the SDPR protein. Bar = 10 μm.

the relationship between these two molecules (Figure 5). Immortalized fibroblasts derived from Cav1$^{-/-}$ mice were transfected with HA–hSRBC alone (Figure 5A and B) and processed for indirect immunofluorescence detection of HA. HA–hSRBC was diffusely distributed in the cytoplasm (Figure 5B) of cells that lack Cav1 (Figure 5A). By contrast, when HA–hSRBC was co-transfected with Cav1–GFP, the two proteins colocalized (Figure 5C and D) and the distribution precisely matched the caveolae staining-pattern usually seen in fibroblasts. Other experiments showed that Cav3–Myc effectively substituted for Cav1 (Figure 5E and F), whereas hSRBC did not colocalize with Cav2–GFP that appeared to have a Golgi apparatus staining pattern (Figure 5G and H). A similar result was obtained with SDPR (data not shown). We conclude that all three members of this family depend on either Cav1 or Cav3 to reach the cell surface.

A requirement for Cav1 in hSRBC targeting to caveolae suggests the two may physically and functionally interact. To test for a physical interaction, we used an immunoprecipitation protocol to see whether the two proteins would reciprocally co-precipitate from solubilized SV589 human fibroblasts. We solubilized the postnuclear supernatant fraction of these cells using a mixture of Triton X-100 and octylglucoside to ensure the complete solubilization of the caveolae, and then we incubated the soluble material with beads containing either α-Cav1 IgG (Figure 5I, left panel) or α-SRBC IgG (Figure 5I, right panel). The beads were washed before the bound proteins were processed for immunoblotting with either α-SRBC IgG (Figure 5I, IB, left panel) or α-Cav1 IgG (Figure 5I, IB, right panel). The immunoblots show that α-Cav1 immunoprecipitated hSRBC and α-SRBC immunoprecipitated Cav1. Therefore, under conditions when both proteins are in caveolae the two proteins are directly or indirectly interacting.

In the tissue survey, we carried out to localize Cav1- and hSRBC-expressing cells (Figure 2), we rarely found Cav1-negative cells that expressed hSRBC. To explore the possible significance of this observation, we used small interfering RNA (siRNA) to reduce the level of Cav1 in fibroblasts (Figure 5J). When we depleted fibroblast Cav1 (lane 1), the amount of hSRBC in the cell markedly declined. A control siRNA did not affect the level of either hSRBC or Cav1 (lanes 2 and 4). By contrast, reducing hSRBC levels did not affect the amount of detectable Cav1 (lane 3). Therefore, the presence of hSRBC appears to be linked to the presence of Cav1, which may explain why we rarely found cells in tissues that expressed hSRBC alone.

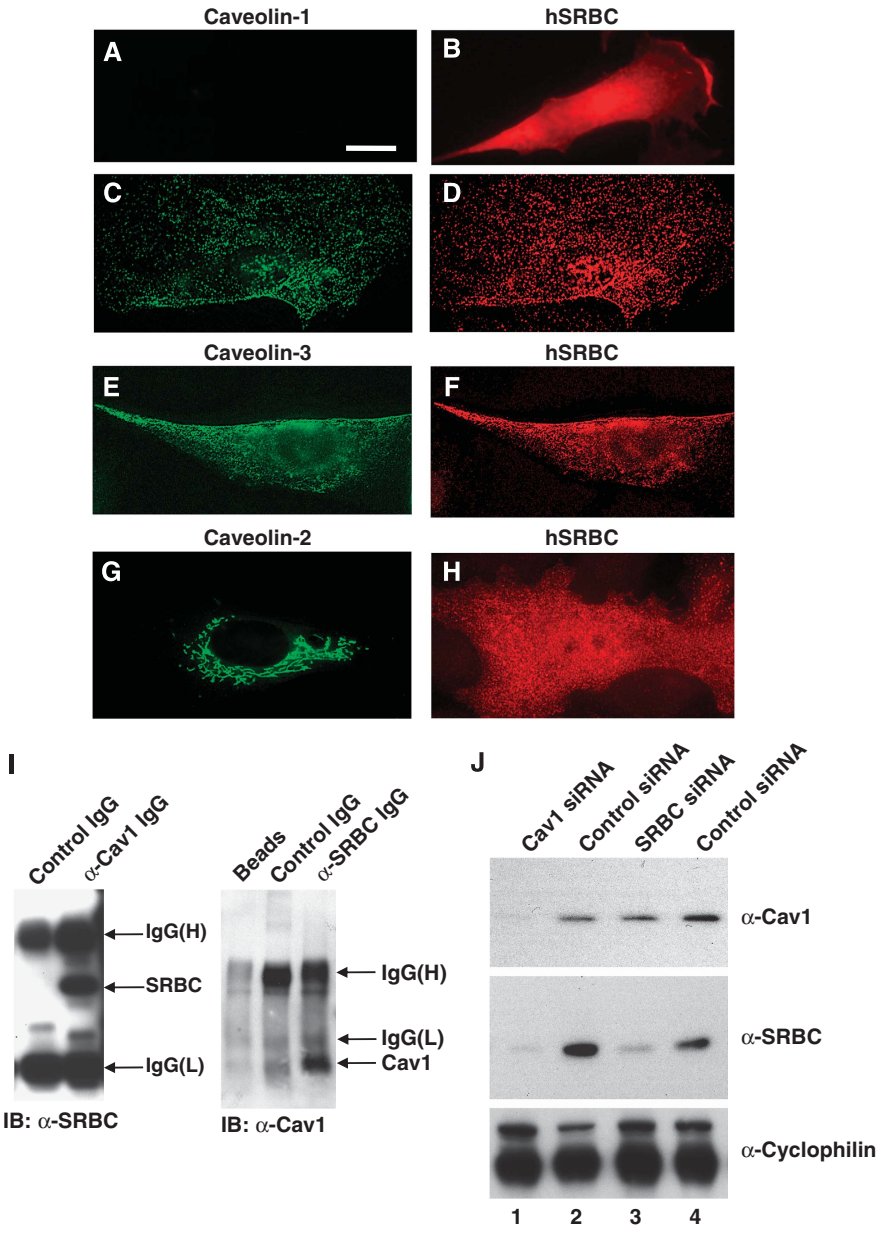

Figure 5 Caveolin-dependent recruitment of hSRBC to caveolae. (**A**, **B**) Mouse Cav1$^{-/-}$ fibroblasts were transiently transfected with HA-tagged hSRBC for 24 h and processed for immunofluorescence colocalization of caveolin (A) and HA (B). (**C**, **D**) Mouse Cav1$^{-/-}$ fibroblasts were transiently co-transfected with cDNAs coding for Cav1–GFP (C) and HA-tagged hSRBC (D) for 24 h, fixed and processed to localize GFP (C) and HA (D). (**E**, **F**) Mouse Cav1$^{-/-}$ fibroblasts were transiently co-transfected with cDNAs coding for Myc–Cav3 and HA-tagged hSRBC for 24 h, fixed and processed for immunofluorescence to localize Myc (E) and HA (F). (**G**, **H**) Mouse Cav1$^{-/-}$ fibroblasts were transiently co-transfected with cDNAs coding for Cav2–GFP and HA-tagged hSRBC for 24 h, fixed and processed for localization of GFP (G) and HA (H). (**I**) The PNS fraction from immortalized human fibroblasts was solubilized with Triton X-100–octylglucosidase and incubated with beads conjugated with pAb α-rabbit IgG (control) or pAb α-caveolin-1 IgG. The beads were washed stringently before the bound proteins were eluted from the beads, separated by SDS–polyacrylamide gel electrophoresis and processed for immunoblotting using mAb α-hSRBC IgG (left panel). Another sample of PNS was processed in the same way substituting mAb α-SRBC for mAb α-Cav1 IgG and immunoblotting with mAb α-Cav1 IgG (right panel). (**J**) Immortalized human fibroblasts were incubated in the presence of siRNAs directed against an irrelevant RNA (lanes 2 and 4), Cav1 RNA (lane 1) and hSRBC RNA (lane 3). After 72 h, the postnuclear supernatant fractions were prepared and processed for immunoblotting using pAb α-Cav1 IgG, mAb α-hSRBC IgG or pAb α-cyclophilin-A IgG as a loading control. Bar = 10 μm.

If the LZ is important for targeting hSRBC to caveolae, then the interaction of Cav1 with ΔLZ–SRBC may be impaired. Immortalized human fibroblasts were transfected with a cDNA coding for HA-tagged WT or ΔLZ–SRBC. The cells were then processed to immunoprecipitate HA and both the immunoprecipitate and the lysate proteins were separated on polyacrylamide gels (Figure 6A). A silver stain of the IP gel shows that the transfected cells express proteins with the molecular weight expected for WT and ΔLZ–SRBC (ΔLZ). The identity of these proteins was verified by immunoblotting (Figure 6B). We noticed in the silver-stained gel of the immunoprecipitates (A) that the WT lane contained high molecular weight (*) and a low molecular weight band (**) that were not present in the control lanes. Mass spectrometry identified the top protein as EPS15R. We confirmed that EPS15R co-precipitated with hSRBC by immunoblotting a

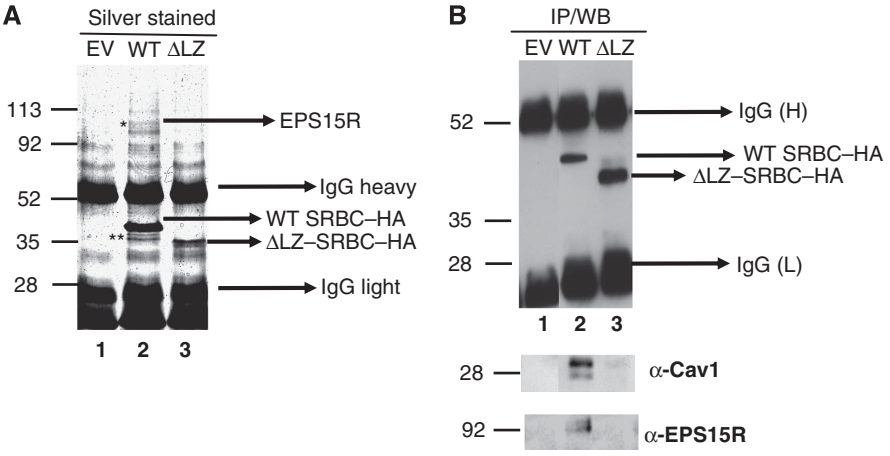

Figure 6 Immunoprecipitation of hSRBC co-precipitates Cav1 and EPS15R. (**A**) The PNS fraction from immortalized human fibroblasts transfected with vectors containing no cDNA (lane 1) or the cDNA for HA-tagged WT hSRBC (lane 2) or the cDNA for HA-tagged Δ22–70 hSRBC was solubilized with a detergent mixture of Triton X-100–octylglucosidase. The solubilized material was incubated with beads conjugated with mAb α-HA IgG. The beads were washed before the bound proteins were processed for separation by polyacrylamide electrophoresis and silver stained. (**B**) The same beads were processed for immunoblotting using α-HA IgG (lanes 1–3) or α-Cav1 IgG (α-Cav1) or α-EPS15R IgG (α-EPS15R).

duplicate gel with antibodies directed against SRBC, Cav1 and EPS15R (Figure 6B, lanes 2 and 3). Cav1 and EPS15R were not present in the immunoprecipitate of ΔLZ–SRBC. Lysates used for the immunoprecipitation contained similar amounts of the expressed (SRBC and ΔLZ–SRBC) as well as endogenous (Cav1 and EPS15R) protein (data not shown).

Cav1 and hSRBC traffic together in cells

Live cell imaging of Cav–GFP has shown that Cav1-rich membranes engage in three types of membrane traffic (types 1–3). To see whether hSRBC traffics with all three types of Cav1-rich membranes, we co-expressed in HeLa cells either hSRBC–tdTomato and Cav1–GFP (Figure 7A–C) or Cav1–tdTomato and hSRBC–GFP (Figure 7D–F) and recorded the behaviour of the two proteins with a spinning disc confocal microscope using excitation at 488 nm (GFP) and 568 nm (tdTomato) and the appropriate band-pass filters to separate the two fluorescence signals (Supplementary Movies S1–S3). In agreement with our immunofluorescence data, hSRBC highly colocalized with caveolin (Figure 7A, yellow), both on the cell surface and on internal vesicles. Live cell imaging detected all three types of caveolin-rich membranes and in each case SRBC was present. Still images of types 1 and 2 caveolae movement are analysed in Figure 7. Type 1 hSRBC/Cav-positive cavicles moved at ~0.8–2.03 μm/s for several micrometres as if travelling along microtubules (Figure 7B and C, still images; Supplementary Movie S1). Interestingly, cavicles displayed saltatory movement (Supplementary Movie S1). They paused 11–33 s (Figure 7A, arrowheads) between segments and often changed direction when movement resumed. Type 2 hSRBC/Cav1-positive cavicles were seen travelling (Supplementary Movie S2) beneath the plasma membrane at an average rate of 2.6 μm/s (Figure 7D–F, arrow and circles). This population of cavicles did not exhibit long pauses nor did they change direction. Type 3 tubular caveolae were also positive for both hSRBC and caveolin (Supplementary Movie S3). These results indicate that hSRBC is intimately associated with caveolae as well as caveolae-derived membranes such as cavicles and caveosomes, and they both remain associated with these membranes as they travel in the cell.

SRBC regulates cavicle traffic

As pointed out earlier, PKCα regulates caveolae internalization (Smart *et al*, 1994, 1995a) and SDPR (also called as SDR) is a candidate caveolar protein responsible for recruiting PKCα to this domain (Mineo *et al*, 1998). We used quantitative EM to see whether reducing the level of SDPR RNA in fibroblasts affects caveolae invagination (Figure 8). Immortalized human fibroblasts (Figure 8A) incubated in the presence of an siRNA against SDPR showed a marked reduction in the number of invaginated caveolae (arrows) compared with cells treated with control siRNA. We quantified the effect of SDPR siRNA in six trials, four for HeLa cells and two for immortalized human cells, by counting the number of invaginated caveola (Figure 8B). SDPR siRNA effectively reduced the amount of SDPR RNA in the cell in each trial. On average, the SDPR siRNA caused ~57% decline in invaginated caveolae in HeLa cells and ~37% in the immortal fibroblast. These results, together with reports that PTRF regulates the number of invaginated caveolae (Hill *et al*, 2008; Liu and Pilch, 2008), suggest that hSRBC might also have a function in the budding and/or traffic of caveolae-rich membranes. Therefore, we set up a fluorescence recovery after photobleaching (FRAP) assay to determine whether hSRBC affects caveolin–GFP traffic.

Previous live cell imaging experiments showed that in CHO cells GFP-positive cavicles in the centrosome region of the cell overlap with recycling endosomes containing transferrin receptors (Mundy *et al*, 2002), and that disrupting microtubules with nocodazole prevented cavicle accumulation at this site (Mundy *et al*, 2002). These experiments suggest that cavicles are dynamically associated with the centrosomal region of the cell. We developed an FRAP assay that allowed us to measure the effect of SRBC on cavicle movement from peripheral sites to the centrosomal region. We photobleached the interior population of caveolin–GFP without bleaching the periphery (Figure 9B), and then monitored the reappearance of individual particles (cavicles) in the centrosomal

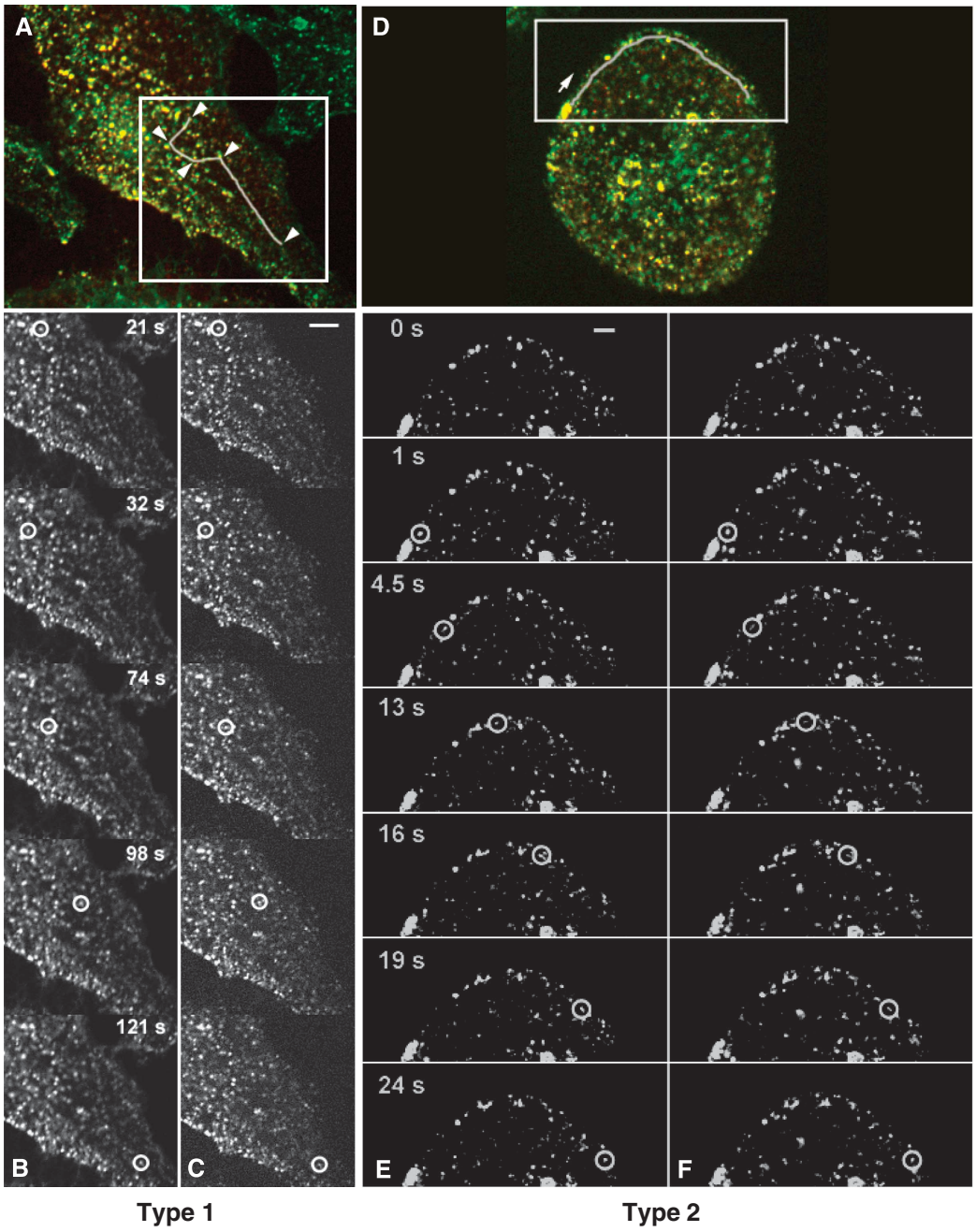

Figure 7 hSRBC and Cav1 traffic together on type 1 and 2 cavicles. A colour composite and individual frames from a time-lapse sequence of HeLa cells co-expressing red SRBC–tdTomato and green Cav1–GFP (see Supplementary Movies S1–S3). (**A**–**C**) The path followed by a single hSRBC–tdTomato/caveolin–GFP-positive type 1 cavicle is traced using Adobe Premiere. The trajectory of the cavicle was divided into four segments. At each of the positions indicated by the arrowheads, the cavicle stopped and hovered on average 19 s (33, 11 and 15 s) before moving on in a new direction. The mean velocity of the moving cavicle, averaged over the four segments, was 1.3 μm/s (1.22, 1.17, 0.8 and 2.03 μm/s). Selected frames from the time-lapse sequence, cropped to the area indicated by the white box in (A). (B) hSRBC–tdTomato; (C) caveolin–GFP. (**D**–**F**) The path followed by a single caveolin–tdTomato/hSRBC–GFP-positive type 2 cavicle is traced using Adobe Premiere. Unlike type 1 cavicles, these cavicles do not pause for significant times and have a trajectory that follows the contour of the membrane. The average speed was 2.6 μm/s. (E) Caveolin–tdTomato; (F) hSRBC–GFP. In each frame, the cavicle being tracked is circled in white. Bar = 5 μm.

region over a 150-s period. Under these conditions, the repopulating cavicles can come either from caveolae that have budded from the plasma membrane or existing cavicles in a remote focal plane of the cell that was not bleached. Particles within the region of interest were identified in each frame of the recovery sequence (Figure 9B, square) using the Spots algorithm of Imaris software (Bitplane, Zurich, SW). The data for each cell was normalized to the baseline number of spots in the first frame obtained after bleaching. The values from approximately 10 cells were averaged for each time point and used to generate a particle reappearance curve (Figure 9C–F). As a positive control for the ability of this assay to detect the cavicle movement, we used HeLa cells expressing caveolin–GFP that had been grown in the presence or absence (Figure 9C, blue diamonds) of either nocodazole (yellow triangle) or genistein (red square). Genistein is a tyrosine kinase inhibitor that blocks caveolae endocytosis (Pelkmans *et al*, 2001). At 120 s after bleaching,

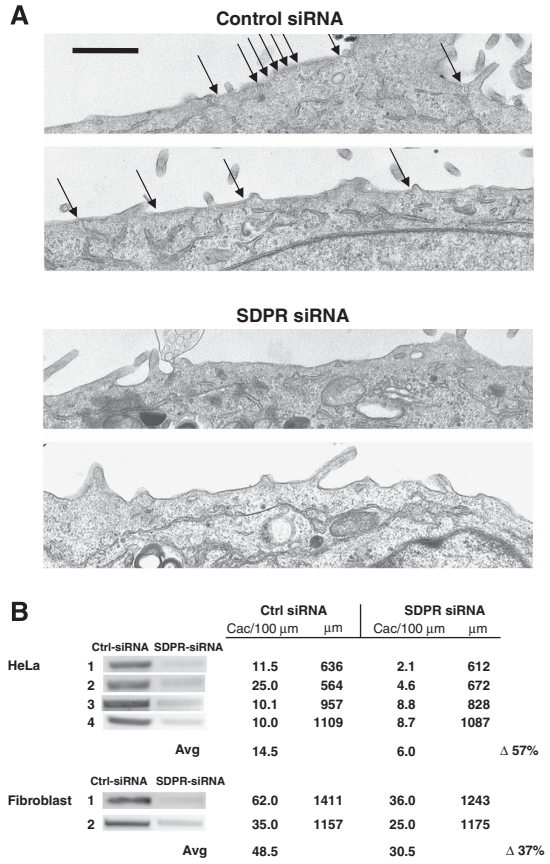

Figure 8 Reducing SDPR in cells correlates with the loss of invaginated caveolae. (**A**) Immortalized human fibroblasts were incubated in the presence of either an siRNA directed against an irrelevant RNA (top two panels) or against SDPR RNA (bottom two panels) and incubated for 48 h before processing samples for thin section EM. Arrows indicate caveolae. Bar = 1 μm. (**B**) The number of caveolae in each sample was quantified by measuring the number of caveolae per micrometre of cell surface. Either HeLa cells (experiments 1–4) or SV40-transformed human fibroblasts (experiments 5 and 6) were incubated in the presence of siRNA directed against the RNA of SDPR (SDPR siRNA) or a sense siRNA (Ctrl-siRNA) for 48 h and the amount of SDPR RNA was detected by PCR. The number of invaginated caveolae in each trial was then measured directly on printed electron micrographs. Averaging four trials for HeLa cells, we saw an ~57% reduction of invaginated caveolae. For human fibroblast, an ~37% loss in SDPR siRNA-treated cells was observed. An observer who did not know the identity of the samples carried out the quantification.

untreated cells had accumulated on average 20 particles in the bleached region. Nocodazole reduced the accumulation to 2.5 particles (seven-fold suppression) and genistein to 10 particles (~2-fold suppression). We conclude that the FRAP assay quantitatively detects cavicle migration to the centrosome and can be used to detect the effect of inhibitors of the process.

We next used the FRAP assay to determine whether hSRBC influences cavicle traffic. We used three non-small cell lung cancer cell lines that express Cav1 but not hSRBC (Sunaga *et al*, 2004). Immunoblots show that these three lines express very little (Figure 9A, lane 3) to no hSRBC (lanes 2 and 4) compared with HeLa cells (lane 1). When any one of these cell types is transfected with a cDNA coding for caveolin–GFP, the GFP signal is found at the cell surface as well as in vesicular structures clustered near the centre of the cell (Figure 9B) just as in HeLa cells. Each of the three cell lines (Figure 9D–F) was co-transfected with caveolin–GFP plus either empty vector (blue squares) or vector containing the cDNA for hSRBC (red squares). Cavicle traffic was then measured using the FRAP method (see Materials and methods). Comparing the three cells, we found that hSRBC-expressing cells exhibited a 2- to 10-fold increase in particle accumulation following photobleaching. This result suggests that hSRBC regulates microtubule-dependent cavicle traffic to the centrosome of these cells.

Discussion

SRBC is the third member of a family of three proteins that have been implicated in regulating caveolae function. Immunofluorescence shows that all of these proteins are selectively concentrated in caveolae, and that an individual caveola can contain more than one member of the family (for example, Supplementary Figure 1S, SDPR and hSRBC). The ability of these proteins to concentrate in caveolae is either directly or indirectly dependent on the expression of Cav1. At least for SDPR and hSRBC, these proteins can associate with both Cav1 and signalling molecules such as PKC. Therefore, SDPR, PTRF and hSRBC appear to have the properties of a caveolin adapter molecule that links signal transduction to the regulation of caveolae function. On the basis of these similar properties, it seems reasonable that the diverse individual names these proteins have acquired over the years be consolidated with the general family name cavin (Vinten *et al*, 2005) and the individual names of cavin-1 (PTRF), cavin-2 (SDPR) and cavin-3 (SRBC).

Cavin-1 and caveolae assembly

Cavin-1/PTRF was originally identified as a factor that stimulated the release of pre-rRNA and Pol I from templates during Pol I-mediated RNA transcription (Jansa *et al*, 1998). Consistent with this function, cavin-1 interacts with the transcription termination factor TTF-1, Pol I, and the 3′ end of pre-rRNA. Cavin-1 has two putative nuclear localization signals (amino acids 143–157 and 196–210) and, in addition to its transcription termination function, can stimulate gene transcription (Jansa *et al*, 1998). Stimulation of transcription has been linked to its RNA releasing activity (Jansa *et al*, 2001). Cavin-1 can also suppress the function of the type I collagen transcription factor BFCOLI (Hasegawa *et al*, 2000), which raises the possibility that it regulates multiple genes.

In the face of these well-documented activities, it is somewhat surprising that in several cell types most of the detectable cavin-1 is in caveolae (Aboulaich *et al*, 2004; Vinten *et al*, 2005; Hill *et al*, 2008; Liu and Pilch, 2008). Moreover, two recent studies (Hill *et al*, 2008; Liu and Pilch, 2008) suggest that cells lacking cavin-1 are defective in caveolae formation. The role of cavin-1 in caveolae assembly has not been determined. It is important to note, however, both studies reported that knocking down cavin-1 in 3T3 L1 cells markedly reduces the level of Cav1 (as much as 75%). Cav1 is thought to be essential for caveolae formation, which raises the possibility that cavin-1 function in part is to control the number and function of surface caveolae by regulating the transcription of the Cav1 gene. Indeed, overexpressing cavin-1 causes a concomitant increase in the amount of Cav1 (Liu and Pilch, 2008). Even if it turns out that cavin-1 regulates

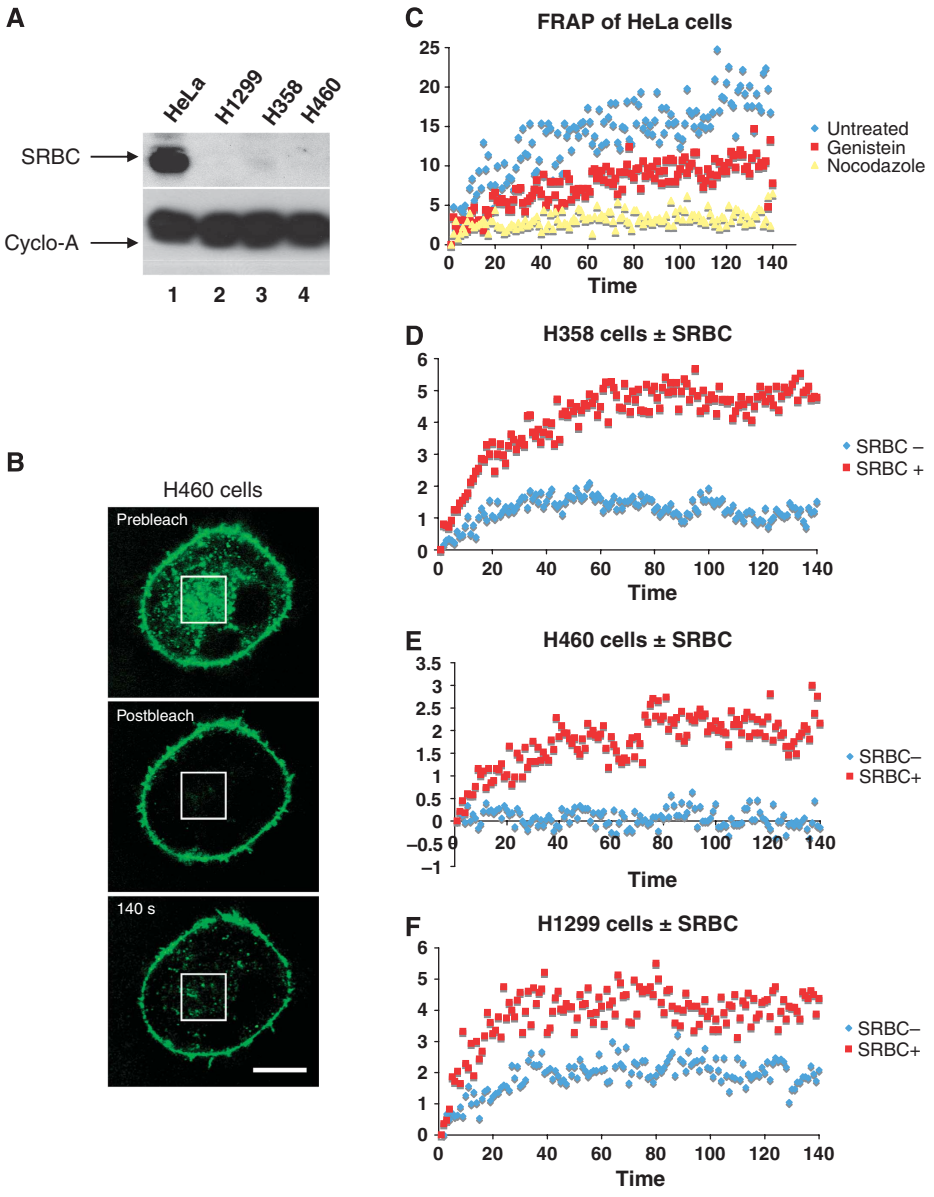

Figure 9 SRBC regulates caveolae traffic. (**A**) The postnuclear supernatant fraction was prepared from HeLa cells, H1299 cells, H358 cells and H460 cells and processed for immunoblotting with mAb α-hSRBC IgG or mAb α-cyclophilin-A IgG as a loading control. (**B**) Three frames from a FRAP sequence showing a H460 cell co-transfected with GFP–Cav1 and full-length wild-type SRBC. The top panel is the frame immediately before beginning photobleaching, the middle panel is the frame immediately after photobleaching and the bottom panel is the frame corresponding to the last time point on the graphs of particle recovery. The white box shows the region where particles were counted using Imaris Spots to generate the data depicted on the graphs. To compensate for the loss of total intensity due to photobleaching over the time course of the recovery, Adobe Photoshop was used to enhance the image in the bottom panel by smoothing it with a Gaussian filter of 0.5 pixel radius to remove shot noise and then rescaling it so that the intensity of the unbleached rim of the cell was comparable to the intensity in the first two panels. Bar = 10 μm. (**C**) HeLa cells transfected with Cav1–GFP were either not treated (blue diamonds), incubated in the presence of 1 μM nocodazole (yellow triangles) or 20 μM genistein (red squares) for 1 h at 37°C. (**D**–**F**) H358, H460 or H1299 cells were co-transfected either with empty vector plus Cav1–GFP (blue diamonds) or with HA-tagged hSRBC and Cav1–GFP (red squares). Cav1–GFP-expressing cells were selected for the FRAP analysis. The region of interest to be photobleached was defined as everything inside the cell excluding the plasma membrane. A single frame was acquired before bleaching with a 488 laser line at full power for up to 25 s. Recovery was recorded for 150 s after photobleaching. For each FRAP time-lapse sequence, a rectangular region at the centrosome was analysed for particle number with time using the Spots module of Imaris (Bitplane). The particle number in the first frame was taken as the baseline. Each time point in Figure 8 is the average particle number from ~10 cells.

the assembly and structure of caveolae directly, there remains the mystery of why a protein with well-established functions in gene regulation is concentrated in caveolae.

Adapter function of cavins

In contrast to cavin-1, there is no direct evidence that either cavin-2/SDPR or cavin-3/SRBC regulates the transcription of Cav1. To the contrary, we found that Cav1 controls the level of cavin-3 in the cell. As these two cavins share with cavin-1 the ability to target caveolae, we focused on identifying a possible adapter function. Adapter proteins regulate the interactions between signalling molecules located in specific cellular compartments. As cavin-2 and 3 are known PKC-binding proteins, a natural place to look for cavin

adapter partner(s) is in caveolae. Mutagenesis experiments showed that targeting of cavin-3 to caveolae was dependent on a four heptad repeat, LZ between amino acids 20 and 76. A three heptad LZ in cavin-2 is also critical for targeting to caveolae, which suggests a general function for LZs in targeting cavins to caveolae. Immunoprecipitation showed that one of the cavin-3-interacting molecules in caveolae is Cav1 and that deleting the LZ blocks this interaction. Another protein that co-precipitated with cavin-3 is EPS15R, which was detected previously in a proteomic analysis of caveolae isolated from adipocytes (Aboulaich *et al*, 2004). We conclude that cavins are adapter proteins that link PKC to regulatory networks involved in controlling caveolae function.

A model protein for understanding how cavin-3 might function is the adapter SLP-65, which is a critical upstream regulator of the B-cell antigen receptor (BCR) (Engelke *et al*, 2007). SLP-65-deficient mice are defective in B-cell development and activation, and they exhibit an increase in pre-B-cell leukaemia. Thus, SLP-65 is a tumour suppressor that increases differentiation and suppresses proliferation of pre-B cells. Cavin-3 has also been reported to be a tumour suppressor. It was isolated in a two-hybrid screen with the first 304 amino acids of BRCA1 and found to be inactive or absent in many breast, lung and ovarian cancer cells (Xu *et al*, 2001). The adapter function of SLP-65 depends on the molecule being at the plasma membrane. Similar to cavin-3, targeting to the cell surface depends on an LZ (Kohler *et al*, 2005). Site-directed substitution of glutamate at L18 and I25 in the LZ converts SLP-65 to a cytosolic protein that is no longer active. Adapter function is restored if a myristoylation consensus sequence is introduced at the N terminus of the LZ-defective protein. LZs, therefore, may have a general function in targeting adapters and other signalling machinery to plasma membrane domains such as caveolae.

Cavin-3 regulates traffic and/or budding of caveolae

Although SLP-65 is intimately involved in regulating the mobilization of cellular Ca^{2+}, the exact signalling pathways regulated by cavins are not clear. Lowering the level of cavin-1 (Hill *et al*, 2008; Liu and Pilch, 2008) or cavin-2 (Figure 8) reduces the number of detectable caveolae. The loss of visible caveolae could be due to a block in the conversion of flat caveolae to invaginated caveolae as occurs when cells are depleted of PKCα (Smart *et al*, 1994), a block in the recycling of caveolae following endocytosis (Mundy *et al*, 2002) or a defect in caveolae assembly (Hill *et al*, 2008; Liu and Pilch, 2008). To assay for cavin-3-dependent functions, we developed an FRAP assay that measures the ability of Cav1–GFP-positive cavicles to repopulate the centrosomal region of the cell where recycling endosomes reside. Repopulation involves type 1 transport of newly budded caveolae to the centrosome (inhibited by both genistein and nocodazole) as well as the arrival of existing cavicles that have travelled on microtubules from different regions of the cell (inhibited by nocodazole alone). We used three lung cancer cell lines that all lack detectable cavin-3. GFP-positive cavicle recovery after photobleaching in these cells is very slow (Figure 9). In each cell type, however, introduction of cavin-3 markedly accelerates the reappearance of cavicles in the centrosome. These experiments suggest that cavin-3 regulates caveolae budding or movement of cavicles along microtubules or both.

These studies suggest that one of the adapter functions of cavin-3, and cavins in general, is to regulate caveolae traffic. Cavin-1 and -2 may regulate caveolae budding, caveolae assembly or both. The assay methods used in these studies cannot distinguish between the two processes. By contrast, Cavin-3 may regulate the migration of cavicles on microtubules. As all three proteins contain PKC-binding motifs and both cavin-2 and -3 have been shown to bind PKCα and PKCδ, respectively, most likely a general function of cavins is to compartmentalize PKC kinase activity in Cav1-rich membranes. Importantly, PKC inhibitors such as staurosporine block endocytosis by caveolae (Mineo and Anderson, 2001; Pelkmans *et al*, 2001). It will be important in future studies to identify the PKC substrates in caveolae, the role of each cavin in targeting the PKC to caveolae and how these substrates function.

Cavin-3 modulation of EGFR targeting to caveolae

The PKC adapter function of cavin-3 may be linked to the targeting of EGFR to caveolae. EGFR was the first receptor tyrosine kinase localized to isolated caveolae (Smart *et al*, 1995b). Subsequent work (Mineo *et al*, 1999) determined that under quiescent conditions EGFR is highly enriched (~7-fold) in caveolae but rapidly departs this domain when the cells are exposed to EGF. EGFR migration from caveolae depends on EGF binding plus a functional tyrosine residue in the regulatory region of the cytoplasmic tail. PKC-dependent phosphorylation of serine 654 markedly reduces EGF-stimulated migration of EGFR from caveolae. Therefore, one way that cavin-3 may affect localization of EGFR to caveolae is by linking PKCδ to the phosphorylation of EGFR.

There is a second way cavin-3 may regulate the concentration of EGFR in caveolae. We found that immunoprecipitates of cavin-3 contain EPS15R, whereas immunoprecipitates of a ΔLZ cavin-3 do not (Figure 6). Immunoprecipitates of Cav1 also contain EPS15R (Hartung *et al*, 2006). EPS15R is a soluble, Ca^{2+}-binding protein related to the EGFR substrate EPS15 that contains multiple EPS15 homology (EH) domains as well as ubiquitin-interacting motifs (UIMs). EH domains have been implicated in regulating endocytosis, vesicle traffic and signal transduction (Carbone *et al*, 1997). Recent studies suggest that EPS15R and the related molecules, EPS15 and epsin, have a critical function in retaining ubiquitinated EGFR in caveolae (Sigismund *et al*, 2005). Ubiquitinated EGFR is enriched in caveolae, and high levels of EGF in the media increase the level of ubiquitinated EGFR. This modified EGFR tends to be internalized by caveolae. By contrast, Y1045F EGFR, which cannot be ubiquitinated, is preferentially internalized by clathrin-coated pits. Therefore, a direct interaction between cavin-3 and the UIMs of EPS15 or EPS15R or epsin may function to regulate the traffic of EGFR to and from caveolae membranes. This model implies that cavin-3 links ubiquitinated EGFR to caveolae, whereas unmodified EGFR, released from caveolae, moves to other membrane domains such as clathrin-coated pits.

Conclusion

Cavins are the first set of caveolae proteins that appear to have adapter functions analogous to the clathrin adapter complexes identified over 20 years ago. Clathrin adapters were first identified by their ability to promote the assembly of clathrin-coated vesicles *in vitro* (Keen *et al*, 1979).

Subsequently, this set of molecules was implicated in a range of activities including attracting membrane receptors to coated pits for internalization (Pearse, 1988). A better understanding of the manner in which cavins work undoubtedly will reveal the full functionality of caveolae and other caveolin-positive membranes.

Materials and methods

Materials

Dulbecco's modified Eagle's medium (DMEM), RPMI 1640, glutamine, trypsin-EDTA were from Sigma (St Louis, MO, USA). Penicillin/streptomycin was from Invitrogen (Carlsbad, CA). Cosmic serum (CS) and fetal bovine serum (FBS) were from HyClone (Logan, UT, USA). pAb α-Cav1 IgG was from BD Bioscience (San Jose, CA). The monoclonal antibody against hSRBC, the full-length HA-tagged hSRBC construct and hSRBC–GFP construct were kindly provided by Dr John Minna (UT Southwestern Medical Center at Dallas, Dallas, TX, USA). Dr Linda Margraf, Department of Pediatrics, UT Southwestern Medical Center, provided samples of human tissue. The tdTomato construct was the generous gift of Dr Roger Tsien (UC San Diego, La Jolla, CA).

Buffer list

Buffer A (PBS), 137 mM NaCl, 10 mM phosphate, 2.7 mM KCl, pH 7.4; buffer B (TBS), 137 mM NaCl, 25 mM Tris–HCl, pH 7.5; buffer C, 3% (w/v) paraformaldehyde in Hank's buffered salt solution containing 20 mM HEPES, 100 mM NaCl, pH 7.3; buffer D, buffer B plus 0.5% Tween-20; buffer E (TETN), 25 mM Tris–HCl, pH 7.5, 5 mM EDTA, 1% Triton X-100, 60 mM octylglucoside plus protease and phosphatase inhibitors; buffer F, 25 mM Tris–HCl, pH 7.5, 5 mM EDTA; buffer G (blocking buffer), buffer D plus 5% dry milk; buffer I (antibody dilution buffer), buffer B plus 0.2% Tween-20 and 1% dry milk; and buffer J (washing buffer), buffer B plus 0.2% Tween-20 and 0.2% dry milk.

Cell culture

SV589 human fibroblasts were cultured in DMEM supplemented with 10% (vol/vol) CS, 100 U/ml penicillin and 100 μg/ml streptomycin. SV589 human fibroblasts were seeded at 1×10^6 cells/ml on day 1 and were routinely used on day 3. Cav1$^{-/-}$ mouse fibroblasts were isolated from the thymus of Cav1 KO mice. The thymus was sliced into very small pieces and cultured in DMEM supplemented with 10% (vol/vol) FBS, 100 U/ml penicillin and 10 μg/ml streptomycin for 1 day. Non-adherent cells were removed from the culture with several washes of medium and then adherent fibroblasts were cultured over 25 passages. These cells were further subcloned to give a clonal population of Cav1$^{+/+}$ and Cav1$^{-/-}$ immortalized fibroblasts.

HeLa cells and non-small cell lung carcinoma cells (H1299, H460 and H358) were obtained from the Hamon Center Collection (UT Southwestern Medical Center at Dallas) and cultured in high glucose DMEM supplemented with 10% (vol/vol) CS, 100 U/ml penicillin and 100 μg/ml streptomycin.

Preparation and transfection of synthetic siRNA

The siRNA sequences against CAV1 (CAV1–1 siRNA) were 5′-CAUCUACAAGCCCAACAATT-3′ (sense) and 5′-GUUGUUGGGCUUGUAGAUGTT-3′ (antisense), against hSRBC (SRBC siRNA) were 5′-GAAGCUCUGCUCCAAAUGG-3′ (sense) and 5′-CCAUUUGGAG CAGAGCUUC-3′ (antisense) and against SDPR (SDPR siRNA) were 5′-CCAUUUCAAAGUGCUCAUCTT-3′ (sense) and 5′-GAUGAGCA CUUUGAAAUGGTT-3′ (antisense). The siRNA target sequences were tested in a BLAST search of GenBank (National Center for Biotechnology Information database) to ensure that only the corresponding gene is the target. RNA oligonucleotides to hSRBC were obtained from the core facility of the University of Texas Southwestern Medical Center and RNA oligonucleotides to Cav1 and SDPR were obtained from Dharmacon RNA Technologies (Lafayette, CO, USA). siRNAs were transfected into cells using oligofectamine transfection reagent (Invitrogen) with a ratio of 6 μl oligofectamine to 400 pmol siRNA. Cells were grown and harvested after 3 days before further analysis. RT–PCR and PCR reaction was performed with Superscript First Strand Synthesis (Invitrogen) with 1 × buffer containing 50 mM $MgCl_2$, 2.5% DMSO, 10 mM dNTP and 10 μM primers in a 40-μl reaction. The primers for detecting hSRBC RNA are (forward) 5′-GGAGCAGAGCGGTCAGGGATC-3′, and (reverse) 5′-GGACCGTTTGAGGTCACTGAC-3′, whereas for SDPR RNA the forward strand was 5′-GTGCAAGAGTTTGTTCTTCAGCCC-3′ and the reverse was 5′-GCCTGAAGAAAGTGGATAGCCTCA-3′. The cycle conditions for hSRBC- and SDPR-specific primers were 75–65°C touchdown (one cycle at 95°C (5 min); 10 touchdown cycles at 94°C (30 s), 75°C (30 s) with a decrease of 1°C each cycle, and at 72°C for 30 s; followed by 30 cycles of 94°C (30 s), 65°C (30 s) and 72°C (30 s), with a final extension at 72°C for 7 min.

Construction of normal and mutant hSRBC cDNA

A series of deletion mutations in hSRBC were generated by PCR from the original cDNA clone of hSRBC using a site-directed mutagenesis kit (Roche, Indianapolis, IN, USA). The resulting hSRBC mutant constructs were confirmed by sequencing. For transient expression of hSRBC mutants, SV589 cells were transiently transfected using Fugene 6 HD reagent (Roche) according to the manufacturer's protocol. The LZ mutant of hSRBC contains a deletion of amino acids 22–70, the putative PS-binding mutant contains a deletion of amino acids 113–124, the PKC-binding mutant contains deletion of amino acids 172–194 and the PEST mutant contains deletion of amino acids 199–247. Cav$^{-/-}$ mouse embryo fibroblasts were transfected by electroporation using the Amaxa MEF kit 1 according to the manufacturer's instructions (Amaxa, Gaithersburg, MD; cat. no. VPD-1004) or by microinjecting cDNAs into the nucleus of individual cells.

Immunofluorescence and immunogold EM

Cells plated onto coverslips in 12-well plates were fixed either with buffer A containing 4% paraformaldehyde at room temperature or with methanol at −20°C. Fixed cells were permeabilized with buffer A containing 0.2% Triton X-100. Nonspecific binding sites were blocked by incubating coverslips for 30 min in buffer A containing 0.5% BSA (Sigma). Fixed cells were incubated with primary antibodies diluted in buffer A containing 0.5% BSA for 1 h, washed with buffer A containing 0.5% BSA several times and then incubated with the appropriate secondary antibodies conjugated to the specified Alexa dyes (Invitrogen) for 1 h before mounting with Aqua Poly Mount (Polysciences Inc., Warrington, PA). Through-focus series of 10–12 optical slices were collected and deconvolved using a Deltavision RT deconvolution microscope (Applied Precision, Issaquah, WA, USA). Pearson coefficients were determined using the colocalization algorithm of either the Deltavision RT software or Imaris. Images presented in Figures 1, 3–5 and 7 were sharpened and contrast enhanced using Adobe Photoshop.

Normal human tissues were fixed in 10% formalin buffered in phosphate and then embedded in paraffin. Paraffin sections (5 mm thick) were de-waxed in three changes of xylene (10 min each) and rehydrated into buffer A. The sections were washed with buffer A containing 50 mM NH_4Cl for 30 min and blocked by incubation for 30 min with buffer B containing 10% (v/v) normal goat serum and 1% (w/v) bovine serum albumin. For double immunofluorescence staining, mAb hSRBC IgG (1:200 dilution) with rabbit anti-Cav1 (10 μg/ml) or non-immune mouse IgG (1:200 dilution) or non-immune rabbit IgG (10 μg/ml) was applied to the coverslips overnight at 4°C. The sections were washed three times in buffer B containing 0.1% BSA. Bound primary antibody was detected by incubation for 2 h with Alexa-Fluor 488-conjugated goat anti-rabbit IgG (10 μg/ml; Molecular Probes, Eugene, OR) and Alexa-Fluor 568-conjugated goat anti-mouse IgG (10 μg/ml). The tissues slides were washed three times in buffer B containing 0.1% BSA, rinsed with water and mounted under a coverslip with Fluorescence Mounting Medium (Dako, Carpinteria, CA). Images were taken using Leica TCS SP confocal microscope.

For EM analysis, cells were processed for indirect immunogold detection of hSRBC (Li *et al*, 2001). Human fibroblasts were cultured in 100-mm dishes to 95% confluence and immersion-fixed in freshly prepared buffer C for 60 min. The cells were enclosed in 2% (w/v) agar and then infused in 2 M sucrose containing 15% (w/v) polyvinylpyrrolidone (10 kDa). Frozen ultrathin sections were prepared using a Leica Ultracut UCT ultramicrotome equipped with a Leica EMFCS cryochamber. The sections were lifted onto nickel grids with infused solution and stored overnight on gelatin at

4°C. Before immunolabelling, the gelatin was liquefied at 37°C, and the nickel grids were removed. We washed the sections by floating them on droplets of buffer A. For immunogold localization, the grids with the attached thin sections were conditioned on droplets of buffer A containing 1% (w/v) bovine serum albumin, 0.01% (v/v) Triton X-100 and 0.01% (v/v) Tween-20 for 10 min at room temperature. The grids were incubated for 2 h in the presence of mouse monoclonal anti-SRBC IgG (1:50 dilution) in buffer A with 0.5% BSA. The sections were rinsed on droplets of buffer A and then incubated with 5-nm gold-labelled goat anti-mouse IgG (diluted 1:40; Amersham Biosciences UK Limited, Little Chalfont, Buckinghamshire, UK) in buffer A with 0.5% BSA. Finally, the grids with the attached thin sections were rinsed in buffer A, fixed with buffer A containing 2% (v/v) glutaraldehyde for 10 min and positive contrast stained (Takizawa and Robinson, 2003). Electron micrographs were taken using a JEOL 1200 electron microscope operating at 80 kV.

Electrophoresis and immunoblotting

Each sample was concentrated by TCA precipitation and washed in acetone. Pellets were suspended in Laemmli sample buffer (Laemmli, 1970), heated at 95°C for 5 min and loaded onto 10% SDS–PAGE. The separated proteins were transferred to PVDF membranes (Millipore, Billerica, MA, USA). The membrane was blocked in buffer G for 1 h at room temperature. Primary antibodies were diluted in buffer I and incubated with the membrane for 1 h at room temperature. The membrane was washed three times for 3 min each in buffer J and incubated with the appropriate HRP-labelled anti-IgG in buffer I for 1 h at room temperature. The membrane was then washed, and the bands were visualized by enhanced chemiluminescence reagent (Amersham Biosciences UK).

Immunoprecipitation

SV589 human fibroblasts were lysed in buffer E plus 150 NaCl for 30 min at 4°C. Lysates were incubated overnight at 4°C with the indicated antibody and protein A-Sepharose CL-4B beads (500 μg of protein; 5 μg of IgG; 50 μl of beads). Immunoprecipitates were washed twice with buffer E containing an additional 250 mM NaCl, twice with buffer E plus 150 mM NaCl and twice in buffer F. Proteins were eluted from beads with SDS sample buffer, separated by SDS–PAGE, transferred to PVDF membrane and blotted with the indicated antibodies.

Spinning disc confocal microscopy

hSRBC–tdTomato was made by inserting hSRBC into the *Hin*dIII/*Eco*RI cut site and tdTomato into the *Xho*I/*Xba*I cut site of pCDNA3.1/V5-His A mammalian expression vector (Invitrogen). Cav1–GFP was constructed as described previously (Mundy *et al*, 2002). The cells were plated in glass-bottomed 35-mm dishes (MatTek Corporation, Ashland, MA) and co-transfected with Cav1–GFP and hSRBC–tdTomato using Fugene (Roche) according to the manufacturer's instructions. At 24–48 h after transfection, fluorescence time-lapse recordings were made at × 63 with a spinning disc confocal microscope (Ultraview ERS; Perkin Elmer, Waltham, MA) using 488- and 568-nm laser lines for excitation and the appropriate band-pass filters to separate the two fluorescence signals. The samples were maintained at 37°C using a stage-mounted heater and an objective heater (Carl Zeiss Microimaging, Thornwood, NY).

FRAP analysis

For FRAP, the cells were plated in glass-bottomed 35-mm dishes (MatTek Corporation). HeLa cells transfected with Cav1–GFP were used for the drug treatment experiments. To examine the role of hSRBC in caveolae trafficking, non-small cell lung carcinoma cells (H358, H460 and H1299), which express Cav1 but not hSRBC as determined by western blotting (Sunaga *et al*, 2004; Xu *et al*, 2001), were obtained from the Hamon Center Collection. The cells were transfected with empty vector and Cav1–GFP cDNA or with WT-SRBC and Cav1–GFP using Fugene (Roche) according to the manufacturer's instructions for 18 h, after which the medium was changed to CO_2-independent medium (cat. no. 18045088; Gibco BRL, Grand Island, NY, USA). Imaging was performed using a Zeiss LSM510 confocal microscope (Carl Zeiss Microimaging). Cells were maintained at 37°C using a stage-mounted heating unit. HeLa cells transfected with Cav1–GFP were left untreated as a control or were treated with 1 μM nocodazole (Sigma) or 20 μM genistein (Calbiochem, San Diego, CA, USA) for 1 h at 37°C. For FRAP, a region of interest containing everything within the boundary of the cell was defined in a single focal plane and fluorescence within the region was bleached with a 488 nm laser line at full power for 30 iterations (about 25 s). *Z*-stacks taken before and after bleaching showed that this protocol typically results in bleaching of fluorescence throughout the thickness of the cell. Recovery was recorded for an additional 150 s after photobleaching at time intervals of 1 s. For the analysis of recovery, a region of interest near the centrosome was defined and the number of GFP-positive particles in this region was analysed for each frame of the time-lapse sequence using the automated spot detection algorithm of Imaris software, setting the minimum particle diameter to 0.2 μm and choosing an intensity threshold (typically <20) that minimized the number of particles in the first frame after photobleaching. The particle number in the first frame after photobleaching was taken as the baseline. Data from 10 cells were combined and the average particle number above baseline in each frame was plotted against frame number.

Mass spectrometry

For proteins that co-precipitated with the WT hSRBC construct and not with an hSRBC construct lacking the LZ (amino acids 22–70), the corresponding silver-stained bands were excised from the gel slab. Each protein band was cut into 1-mm pieces, and destained in 25 mM NH_4HCO_3, 50% methanol, 50% water three times for 10 min. They were washed with equal volumes of 10% acetic acid, 50% methanol, 40% water three times for 1 h, and swollen in water twice for 20 min. The gel pieces were dehydrated with ACN and dried in SpeedVac (Thermo Savant, Holbrook, NY, USA). The gel pieces were again rehydrated with modified porcine trypsin (Promega, Madison, WI, USA) at a concentration of 10 ng/ml in 50 mM NH_4HCO_3 and then subjected to trypsin proteolytic digestion at 37°C overnight. Tryptic peptides were sequentially extracted with an equal volume mixture of 50% ACN, 45% water and 5% TFA followed by an equal volume mixture of 75% ACN, 24.9% water and 0.1% TFA. The peptide extracts were combined and dried in SpeedVac. The peptide samples were cleaned with ZipTip C18 (Millipore) prior to HPLC-MS/MS analysis. HPLC-MS/MS analysis and protein sequence identification were performed as described previously (McMahon *et al*, 2006).

Supplementary data

Supplementary data are available at *The EMBO Journal* Online (http://www.embojournal.org).

Acknowledgements

We thank Jason Hall and Daniel Epstein for their valuable technical assistance and Brenda Pallares for administrative assistance. Confocal and deconvolution microscopy were carried out with the assistance of the UT Southwestern Live Cell Imaging Core Facility. Yun-shu Ying did the EM quantification of caveolae. This study was supported by grants from the National Institutes of Health (HL 20948, GM 52016 and P50CA70907), the Department of Defense (DOD VITL), the Perot Family Foundation, the Sarah M & Charles E Distinguished Chair in Cancer Research, the Max L Thomas Distinguished Chair in Molecular Pulmonary Oncology and the Cecil H Green Distinguished Chair in Cellular and Molecular Biology.

References

Aboulaich N, Ortegren U, Vener AV, Stralfors P (2006) Association and insulin regulated translocation of hormone-sensitive lipase with PTRF. *Biochem Biophys Res Commun* **350:** 657–661

Aboulaich N, Vainonen JP, Stralfors P, Vener AV (2004) Vectorial proteomics reveal targeting, phosphorylation and specific fragmentation of polymerase I and transcript release factor (PTRF) at the surface of caveolae in human adipocytes. *Biochem J* **383:** 237–248

Anderson RG, Kamen BA, Rothberg KG, Lacey SW (1992) Potocytosis: sequestration and transport of small molecules by caveolae. *Science* **255:** 410–411

Carbone R, Fre S, Iannolo G, Belleudi F, Mancini P, Pelicci PG, Torrisi MR, Di Fiore PP (1997) eps15 and eps15R are essential components of the endocytic pathway. *Cancer Res* **57:** 5498–5504

Chang WJ, Ying YS, Rothberg KG, Hooper NM, Turner AJ, Gambliel HA, De Gunzburg J, Mumby SM, Gilman AG, Anderson RG (1994) Purification and characterization of smooth muscle cell caveolae. *J Cell Biol* **126:** 127–138

Chapline C, Cottom J, Tobin H, Hulmes J, Crabb J, Jaken S (1998) A major, transformation-sensitive PKC-binding protein is also a PKC substrate involved in cytoskeletal remodeling. *J Biol Chem* **273:** 19482–19489

Costes SV, Daelemans D, Cho EH, Dobbin Z, Pavlakis G, Lockett S (2004) Automatic and quantitative measurement of protein–protein colocalization in live cells. *Biophys J* **86:** 3993–4003

Engelke M, Engels N, Dittmann K, Stork B, Wienands J (2007) Ca(2+) signaling in antigen receptor-activated B lymphocytes. *Immunol Rev* **218:** 235–246

Hartung A, Bitton-Worms K, Rechtman MM, Wenzel V, Boergermann JH, Hassel S, Henis YI, Knaus P (2006) Different routes of bone morphogenic protein (BMP) receptor endocytosis influence BMP signaling. *Mol Cell Biol* **26:** 7791–7805

Hasegawa T, Takeuchi A, Miyaishi O, Xiao H, Mao J, Isobe K (2000) PTRF (polymerase I and transcript-release factor) is tissue-specific and interacts with the BFCOL1 (binding factor of a type-I collagen promoter) zinc-finger transcription factor which binds to the two mouse type-I collagen gene promoters. *Biochem J* **347** (Part 1)**:** 55–59

Hill MM, Bastiani M, Luetterforst R, Kirkham M, Kirkham A, Nixon SJ, Walser P, Abankwa D, Oorschot VM, Martin S, Hancock JF, Parton RG (2008) PTRF-Cavin, a conserved cytoplasmic protein required for caveola formation and function. *Cell* **132:** 113–124

Isshiki M, Ying YS, Fujita T, Anderson RG (2002) A molecular sensor detects signal transduction from caveolae in living cells. *J Biol Chem* **277:** 43389–43398

Izumi Y, Hirai S, Tamai Y, Fujise-Matsuoka A, Nishimura Y, Ohno S (1997) A protein kinase Cdelta-binding protein SRBC whose expression is induced by serum starvation. *J Biol Chem* **272:** 7381–7389

Jaken S, Parker PJ (2000) Protein kinase C binding partners. *Bioessays* **22:** 245–254

Jansa P, Burek C, Sander EE, Grummt I (2001) The transcript release factor PTRF augments ribosomal gene transcription by facilitating reinitiation of RNA polymerase I. *Nucleic Acids Res* **29:** 423–429

Jansa P, Grummt I (1999) Mechanism of transcription termination: PTRF interacts with the largest subunit of RNA polymerase I and dissociates paused transcription complexes from yeast and mouse. *Mol Gen Genet* **262:** 508–514

Jansa P, Mason SW, Hoffmann-Rohrer U, Grummt I (1998) Cloning and functional characterization of PTRF, a novel protein which induces dissociation of paused ternary transcription complexes. *EMBO J* **17:** 2855–2864

Keen JH, Willingham MC, Pastan IH (1979) Clathrin-coated vesicles: isolation, dissociation and factor-dependent reassociation of clathrin baskets. *Cell* **16:** 303–312

Kohler F, Storch B, Kulathu Y, Herzog S, Kuppig S, Reth M, Jumaa H (2005) A leucine zipper in the N terminus confers membrane association to SLP-65. *Nat Immunol* **6:** 204–210

Laemmli UK (1970) Cleavage of structural proteins during the assembly of the head of bacteriophage T4. *Nature* **227:** 680–685

Lee JH, Byun DS, Lee MG, Ryu BK, Kang MJ, Chae KS, Lee KY, Kim HJ, Park H, Chi SG (2007) Frequent epigenetic inactivation of hSRBC in gastric cancer and its implication in attenuated p53 response to stresses. *Int J Cancer* **122:** 1573–1584

Li WP, Liu P, Pilcher BK, Anderson RG (2001) Cell-specific targeting of caveolin-1 to caveolae, secretory vesicles, cytoplasm or mitochondria. *J Cell Sci* **114:** 1397–1408

Liu L, Pilch PF (2008) A critical role of cavin (polymerase I and transcript release factor) in caveolae formation and organization. *J Biol Chem* **283:** 4314–4322

McMahon KA, Zhu M, Kwon SW, Liu P, Zhao Y, Anderson RG (2006) Detergent-free caveolae proteome suggests an interaction with ER and mitochondria. *Proteomics* **6:** 143–152

Mineo C, Anderson RG (2001) Potocytosis. Robert Feulgen Lecture. *Histochem Cell Biol* **116:** 109–118

Mineo C, Anderson RG, White MA (1997) Physical association with ras enhances activation of membrane-bound raf (RafCAAX). *J Biol Chem* **272:** 10345–10348

Mineo C, Gill GN, Anderson RG (1999) Regulated migration of epidermal growth factor receptor from caveolae. *J Biol Chem* **274:** 30636–30643

Mineo C, James GL, Smart EJ, Anderson RG (1996) Localization of epidermal growth factor-stimulated Ras/Raf-1 interaction to caveolae membrane. *J Biol Chem* **271:** 11930–11935

Mineo C, Ying YS, Chapline C, Jaken S, Anderson RG (1998) Targeting of protein kinase Calpha to caveolae. *J Cell Biol* **141:** 601–610

Mundy DI, Machleidt T, Ying YS, Anderson RG, Bloom GS (2002) Dual control of caveolar membrane traffic by microtubules and the actin cytoskeleton. *J Cell Sci* **115:** 4327–4339

Parton RG, Way M, Zorzi N, Stang E (1997) Caveolin-3 associates with developing T-tubules during muscle differentiation. *J Cell Biol* **136:** 137–154

Pearse BM (1988) Receptors compete for adaptors found in plasma membrane coated pits. *EMBO J* **7:** 3331–3336

Pelkmans L, Kartenbeck J, Helenius A (2001) Caveolar endocytosis of simian virus 40 reveals a new two-step vesicular-transport pathway to the ER. *Nat Cell Biol* **3:** 473–483

Pelkmans L, Zerial M (2005) Kinase-regulated quantal assemblies and kiss-and-run recycling of caveolae. *Nature* **436:** 128–133

Peters PJ, Mironov AJ, Peretz D, van Donselaar E, Leclerc E, Erpel S, DeArmond SJ, Burton DR, Williamson RA, Vey M, Prusiner SB (2003) Trafficking of prion proteins through a caveolae-mediated endosomal pathway. *J Cell Biol* **162:** 703–717

Sigismund S, Woelk T, Puri C, Maspero E, Tacchetti C, Transidico P, Di Fiore PP, Polo S (2005) Clathrin-independent endocytosis of ubiquitinated cargos. *Proc Natl Acad Sci USA* **102:** 2760–2765

Smart EJ, Foster DC, Ying YS, Kamen BA, Anderson RG (1994) Protein kinase C activators inhibit receptor-mediated potocytosis by preventing internalization of caveolae. *J Cell Biol* **124:** 307–313

Smart EJ, Ying YS, Anderson RG (1995a) Hormonal regulation of caveolae internalization. *J Cell Biol* **131:** 929–938

Smart EJ, Ying YS, Mineo C, Anderson RG (1995b) A detergent-free method for purifying caveolae membrane from tissue culture cells. *Proc Natl Acad Sci USA* **92:** 10104–10108

Sunaga N, Miyajima K, Suzuki M, Sato M, White MA, Ramirez RD, Shay JW, Gazdar AF, Minna JD (2004) Different roles for caveolin-1 in the development of non-small cell lung cancer versus small cell lung cancer. *Cancer Res* **64:** 4277–4285

Tahira T, Ochiai M, Hayashi K, Nagao M, Sugimura T (1987) Activation of human c-raf-1 by replacing the N-terminal region with different sequences. *Nucleic Acids Res* **15:** 4809–4820

Takizawa T, Robinson JM (2003) Ultrathin cryosections: an important tool for immunofluorescence and correlative microscopy. *J Histochem Cytochem* **51:** 707–714

Thomsen P, Roepstorff K, Stahlhut M, van Deurs B (2002) Caveolae are highly immobile plasma membrane microdomains, which are not involved in constitutive endocytic trafficking. *Mol Biol Cell* **13:** 238–250

Vinten J, Johnsen AH, Roepstorff P, Harpoth J, Tranum-Jensen J (2005) Identification of a major protein on the cytosolic face of caveolae. *Biochim Biophys Acta* **1717:** 34–40

Voldstedlund M, Thuneberg L, Tranum-Jensen J, Vinten J, Christensen EI (2003) Caveolae, caveolin and cav-p60 in smooth muscle and renin-producing cells in the rat kidney. *Acta Physiol Scand* **179:** 179–188

White MA, Anderson RG (2005) Signaling networks in living cells. *Annu Rev Pharmacol Toxicol* **45:** 587–603

Xu XL, Wu LC, Du F, Davis A, Peyton M, Tomizawa Y, Maitra A, Tomlinson G, Gazdar AF, Weissman BE, Bowcock AM, Baer R, Minna JD (2001) Inactivation of human SRBC, located within the 11p15.5–p15.4 tumor suppressor region, in breast and lung cancers. *Cancer Res* **61:** 7943–7949

Zochbauer-Muller S, Fong KM, Geradts J, Xu X, Seidl S, End-Pfutzenreuter A, Lang G, Heller G, Zielinski CC, Gazdar AF, Minna JD (2005) Expression of the candidate tumor suppressor gene hSRBC is frequently lost in primary lung cancers with and without DNA methylation. *Oncogene* **24:** 6249–6255